

Physical Characterization of Icosahedral Virus Ultra Structure, Stability, and Integrity Using Electrospray Differential Mobility Analysis

Leonard F. Pease III,^{*,†,‡} De-Hao Tsai,^{†,§} Kurt A. Brorson,[⊥] Suvajyoti Guha,^{†,§} Michael R. Zachariah,^{†,§} and Michael J. Tarlov^{*,†}

[†]National Institute of Standards and Technology (NIST), 100 Bureau Drive, Gaithersburg, Maryland 20899, United States

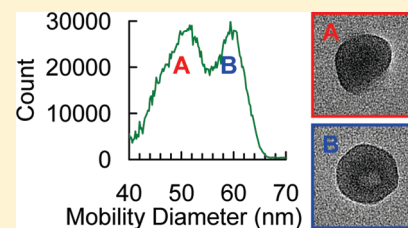
[‡]Departments of Chemical Engineering, Pharmaceutics and Pharmaceutical Chemistry, and Internal Medicine, The University of Utah, Salt Lake City, Utah 84112, United States

[§]Departments of Chemistry and Mechanical Engineering, The University of Maryland, College Park, Maryland 20742, United States

[⊥]Center for Drug Evaluation and Research, Food and Drug Administration, Silver Spring, Maryland 20903, United States

Supporting Information

ABSTRACT: We present a rapid and quantitative method to physically characterize the structure and stability of viruses. Electrospray differential mobility analysis (ES-DMA) is used to determine the size of capsomers (i.e., hexons) and complete capsids. We demonstrate how to convert the measured mobility size into the icosahedral dimensions of a virus, which for PR772 become 68.4 nm for vertex-to-vertex, 54.4 nm for facet-to-facet, and 58.2 nm for edge-to-edge lengths, in reasonable agreement with dimensions from transmission electron microscopy for other members of the family *Tectiviridae* (e.g., PRD1). These results indicate ES-DMA's mobility diameter most closely approximates the edge-to-edge length. Using PR772's edge length (36.0 nm) and the size of the major capsid hexon (≈ 8.4 nm) from ES-DMA with icosahedral geometry, PR772's $T = 25$ symmetry is confirmed and the number of proteins in the capsid shell is determined. We also demonstrate the use of ES-DMA to monitor the temporal disintegration of PR772, the thermal degradation of PP7, and the appearance of degradation products, essential to viral stability assays. These results lay groundwork essential for the use of ES-DMA for a variety of applications including monitoring of vaccine and gene therapy vector products, confirmation of viral inactivation, and theoretical studies of self-assembling macromolecular structures.



Determining the structure, composition, and integrity of viruses, viral vectors for gene therapy and virus-like particles is essential to assuring the quality of vaccines and gene therapy products during their development and manufacture.¹ However, determining viral structure and integrity can be challenging and expensive using state-of-the-art techniques (e.g., X-ray crystallography and cryoelectron microscopy), leaving structural databases (e.g., the International Committee on Taxonomy of Viruses (ICTV) database) incomplete, particularly for recently discovered or less studied viral species. Here, we hypothesize that an emerging technique, electrospray differential mobility analysis (ES-DMA), can be used to interrogate viral structure and stability. ES-DMA is particularly attractive because it is rapid (analysis time on the order of 1 h), the required capital equipment is modest in cost and dimensions, and time-consuming crystallization is not required.

Despite the importance of viral structure, there are few methods capable of quantifying and validating it. The most common technique to determine viral structure is X-ray crystallography,^{1,2} which provides atomic resolution. However, this method is costly and requires extensive computational resources. Furthermore, formation of suitably large crystals is often difficult and, in some cases,

prevents structural determination with this technique. Alternatively, cryo-electron microscopy (cryo-EM) may be used to ascertain viral structure. This technique also boasts atomic scale resolution, and many viruses in the Virus Particle Explorer (VIPER) database have been determined using cryo-EM. Drawbacks of the method include the low temperatures required to prevent electron beam damage to the sample and its expense, which limits availability. More recently, other techniques including small angle neutron scattering (SANS) have become available to determine structure, but this technique, too, suffers from limited availability.³ With each of these techniques, only a small portion of the structure (e.g., individual proteins) is typically determined. The entire structure is then built up or assembled from the smaller components much like the virus itself. Time of flight mass spectrometry (TOF-MS) can similarly be used to determine the number of proteins per virus and, when coupled with low pressure ion mobility spectroscopy, provides information regarding structural intermediates.⁴ Transmission electron microscopy (TEM) is also a workhorse for virus

Received: November 15, 2010

Accepted: January 7, 2011

Published: February 08, 2011

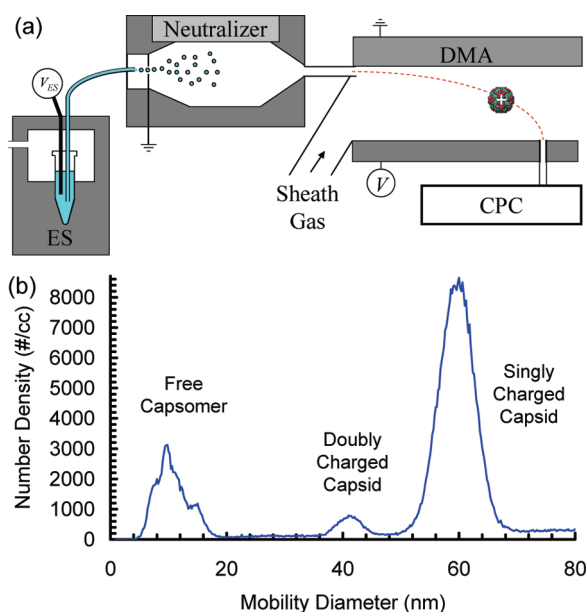


Figure 1. (a) Schematic depicting the major components of the analysis system: electro-spray (ES) and neutralizer to set the charge on the dry protein, a differential mobility analyzer (DMA) to separate and collect particles by their size-to-charge ratio determined trajectory, and a condensation particle counter (CPC) to enumerate the particles. (b) Typical size distribution of positively charged PR772 showing both intact capsid and free capsomers with data collected every 0.2 nm.

measurement with most entries in the ICTV determined by this technique.

Here, we demonstrate the utility of electro-spray differential mobility analysis (ES-DMA) for rapid and quantitative characterization of the structure and physical integrity of viruses.⁵ This complementary technique can determine virus ultrastructure using a “top-down” strategy as opposed to “bottom-up” approaches in common use. While ES-DMA does not possess the atomic scale resolution of X-ray crystallography, cryo-EM, or SANS, its simplicity gives it decided advantages in speed and cost, and the “coarse-grain” structures it provides can provide significant information regarding the structure and assembly of viruses, virus-like particles, and vaccines for biomedical and biomanufacturing applications. Figure 1a shows the components of the instrumentation, and a more thorough description of the instrumentation and operating conditions can be found elsewhere and in the Supporting Information.^{6,7} The distributions reported herein were obtained in less than 100 min on a research grade instrument, and instruments optimized for speed can obtain similar distributions an order of magnitude faster.⁸ The ES-DMA system is ideally suited for studies of viruses as it can analyze particles as small as 3 nm and as large as 700 nm.

ES-DMA has been previously used to measure the size of both large and small viruses including adenovirus (including strain MAD-K87),^{9,10} rhinovirus (HRV2 and HRV14),^{10,11} rice yellow mottle virus (RYMV),^{9,10} cowpea mosaic virus (CPMV),¹⁰ MS2,^{3,9–12} cowpea chlorotic mottle virus (CCMV),¹³ reo-3 reovirus,⁹ and the Kilham rat virus (KRV).⁹ Viruses with tubular components such as T2, T4, λ -phage,¹² and tobacco mosaic virus (TMV)¹⁴ have also been analyzed. Lute et al.⁵ and Wick et al.⁹ extended this technique to viruses of interest to biomanufacturers by characterizing the size distributions of murine minute virus (MVM, parvovirus) and the biosafety level 1 (BSL1) models,

pp7 and ϕ X174, used in virus filtration studies.^{5,9} Recently, Pease et al. incorporated 17 amino acid residues of the H5N1 hemagglutinin residue into surface loops of the murine polyoma virus to generate virus-like particles with vaccine applications and compared ES-DMA size distributions to those of TEM and asymmetric flow field flow fractionation to find good agreement among the techniques.¹⁵

Although sample integrity is a concern with electro-spray, ES-DMA has been demonstrated to be gentle for both protein complexes and enveloped viruses. Indeed, a highlight of the work by Wick and co-workers is their analysis of the enveloped viruses alpha virus (*Togaviridae*), murine hepatitis virus (MHV, *Coronaviridae*), and sendai rodent virus (*Paramyxoviridae*).⁹ For example, ES-DMA measured the alpha virus to be 70 nm \pm 3 nm, in good agreement with the ICTV values of 70 nm (whereas the nucleocapsid diameter is 40 nm).⁹ This agreement indicates that the electro-spray and neutralizer are sufficiently gentle to preserve the lipid envelop despite shear forces present in the Taylor Cone at exit of the electro-spray capillary. Furthermore, Hogan et al. and Siuzdak et al. have shown that icosahedral viruses remain infectious following electro-spray.^{12,16} However, some degradation has been observed in the work of Wick et al.⁹ Here, we systematically vary the extent of degradation to determine viral stability.

Previous ES-DMA studies of viruses reported only the mobility diameter, neglecting the inherent geometry of the virus.^{5,10,12,17} Here, we demonstrate the use of ES-DMA to determine the icosahedral dimensions of viruses. We first review briefly the physics behind the technique and identify the primary capsid peaks in the size distribution, allowing determination of the symmetry (i.e., the *T* number) and the number of major capsid proteins per capsid. We demonstrate how to identify the capsomers and capsomer assemblies by calculating the mobility size through projected area by averaging¹⁸ coordinates from the protein data bank. We finally conclude by determining the temporal degradation of capsids and their half-life and explore thermal degradation mechanisms. The method described here may be extended to a wide variety of icosahedral virus structures.

MATERIALS AND METHODS

Note: Reference to commercial equipment, supplies, or software neither implies its endorsement by the National Institute of Standards and Technology (NIST) or the FDA nor implies that it is necessarily best suited for this purpose.

Coliphage PR772 and host *E. coli* strain K-12 J53.1 were obtained from the Félix d'Hérelle Reference Center for Bacterial Viruses (Université Laval, Québec, Canada). Stocks were prepared by CsCl gradient ultracentrifugation methods as described elsewhere.^{19,20} “Live”, intact phages were enumerated by a plaque assay at 3.7×10^{11} pfu/mL. The phages were then dialyzed through a membrane with a 10 kDa molecular weight cut off into 2.0 mmol/L ammonium acetate (pH 8.13) in preparation for the electro-spray, which requires removal of nonvolatile salts and tuning of the conductivity for optimal electro-spray operation. Removal of these salts also prevents skewing of the size measurement.^{6,21} For room temperature thermal degradation experiments, a single PR772 sample was placed on a countertop at room temperature (approximately 20–25 °C) for the duration of the experiment. This PR772 solution was sampled repeatedly to obtain the size distributions reported.

For thermal degradation at elevated temperatures, the phage PP7 and its host *Pseudomonas aeruginosa* were obtained from the ATCC (Manassas, VA; accession numbers 15692-B4 and 15692).

Stocks were prepared by CsCl gradient ultracentrifugation methods as described elsewhere.^{5,20} The initial titer was 6.9×10^{12} pfu/mL. The phages were dialyzed into 10 mmol/L ammonium acetate, pH 7, in preparation for electrospraying. These samples were then heated to temperatures from 50 to 80 °C by heating to the desired temperature for 30 min following a 4–7 min ramp. After reaching temperature, the variation remained within the range of ± 1.5 °C as measured by a type K thermocouple inserted directly into sample vials via holes punctured through their caps. After 30 min, the samples were removed from the heater. Control samples for comparison were held at ambient temperature (≈ 25 °C) for 30 min. For infectivity loss experiments, highly concentrated phage in 10 mmol/L tris, pH 7.5, was diluted 1:100 into PBS, pH 7.0, or 10 mmol/L ammonium acetate, pH 7.0. The diluted phage solution was heated in screw-cap microcentrifuge tubes by placing them in an adjustable temperature water bath set at various temperatures for 30 min. The temperature of the water bath was verified by a thermometer. “Live” phages in the resulting test articles were enumerated by a plaque assay. Dilutions of the virus stocks and heat treated samples were prepared and added to midlog phase host and liquefied top agar, which was spread over tryptic soy agar plates. Because the infectious titer of active virus can change by several orders of magnitude across a unit operation, common parlance in the industry expresses the infectious titer change in base 10 logarithms. This change is termed the log reduction value or LRV and defined as

$$\text{LRV} \equiv \log_{10} \left(\frac{N_{\text{in}}}{N_{\text{out}}} \right) = \log_{10} \left(\frac{C_{\text{in}} V_{\text{in}}}{C_{\text{out}} V_{\text{out}}} \right) \quad (1)$$

where N_{in} , C_{in} , and V_{in} are the virus particle count, concentration, and volume at the beginning of a batch degradation process and N_{out} , C_{out} , and V_{out} are the virus particle count, infectious titer, and volume at the end.

Within the ES-DMA, the protein particles (capsomers, intact capsid, etc.) are first aerosolized and charged (please see Supporting Information for additional description). The net charge on the protein is acquired in the electrospray, which produces highly charged droplets, and a subsequent charge neutralizer, which reduces the charge to a modified Boltzmann distribution.^{17,18} As a result, the majority of positively charged particles analyzed by DMA possess a single positive charge once the droplet dries, though a few are doubly charged. The DMA is similar to mass spectrometry except that it operates near atmospheric pressure. Within the annular DMA chamber, a flow of nitrogen gas drags the protein particles (capsomers, intact capsid, etc.) along, while the positively charged viruses are attracted to a negatively biased, central electrode. Only particles with the right trajectory, determined by balancing electrical and drag forces acting on them, enter a fixed collection slit to be counted with a condensation particle counter.²² Consequently, separation occurs based on the size-to-charge ratio of the particle. Systematically stepping through potentials ranging from 0 kV to -10 kV affects the trajectory of the viruses, yielding size distributions over a wide size-to-charge range. The mobility size ratio reported in Figure 1b assumed the particles to be spheres, though our analysis below draws on pioneering work by Epstein²³ and later Dahneke²⁴ who showed that the drag force on particles smaller than the mean free path of the surrounding gas scales with the projected area of the particle.

To correlate the mobility size with the dimension of an icosahedron, we use the projected area formalism established by Pease et al.^{6,18,25} Their expressions require that the projected areas be selected perpendicular to the principle axes chosen from fluid dynamics considerations.¹⁸ To determine the influence of errors in this selection process, we rotated an icosahedron about an axis. The projected areas were determined by subdividing the projection into triangles and calculating their area using Heron’s formula, which depends exclusively on the edge lengths. These lengths were determined by taking the Euclidean distances between neighboring vertices in the projection. Rotation introduces at most 0.43% uncertainty in the prediction of the mobility diameter.

RESULTS AND DISCUSSION

We now describe the identification of capsomers and capsomer assemblies in ES-DMA size distributions and how to extract structural information from these data. These methods are then used as a basis to determine the stability and integrity of virus samples and identify degradation mechanisms using ES-DMA.

Figure 1b shows a typical mobility size distribution for PR772, a member of the family *Tectiviridae*. We selected PR772 for this work because it can be grown to high titer, is noninfectious in humans, and thus, can be analyzed safely in a BSL 1 environment.¹⁹ Retention of PR772 has also been used to standardize large virus retentive filter studies; it serves as a model for large mammalian viruses including retroviruses and adenovirus.¹⁹ The larger peaks (>30 nm) represent the completely intact virus. We find the number-average mobility diameter to be 59.6 ± 0.6 nm (1σ on the triplicately measured number-average diameter). This value is in reasonable agreement with the size of other members of the family *Tectiviridae* determined by electron microscopy.²⁶ For example, the size of bacteriophage PRD1, another member of *Tectiviridae* with a 97.2% similar genome, has been measured at 63 nm.^{19,27} The major capsid protein of PRD1, P3 ($M_w = 47.4$ kDa), has a molecular weight that differs from the equivalent PR772 protein by less than 0.06% ($M_w = 47.5$ kDa), and the remaining capsid proteins, such as the receptor binding protein P2, possess marginally larger molecular weights than the equivalent PR772 proteins.¹⁹ Therefore, a similar but slightly smaller size for PR772 would not be unexpected. The peak width, ± 3.1 nm (1σ), includes contributions from instrument uncertainty (2.5 nm),²² Brownian translation within the DMA chamber,²⁸ and protein flexibility, *inter alia*.²⁹

Previous ES-DMA studies of viruses reported only the mobility diameter, neglecting the inherent geometry of the virus.^{5,10,12,17} This left the connection between mobility and actual dimensions of the virus unclear and poorly defined. Here, we convert the mobility diameter, d_m , into the icosahedral geometry expected of *Tectiviridae* using the projected area formalism introduced by Pease et al., to explain the packing of nanoparticle clusters.¹⁸ The drag force in the free molecular flow regime scales on the projected area. Within the DMA chamber, nitrogen molecules that collide with the capsid away from its center of mass induce Brownian rotation, which leads to the following average mobility diameter:

$$d_m = \left(\frac{\sqrt{\pi}}{6} \sum_{i=1}^3 A_i^{-1/2} \right)^{-1} \quad (2)$$

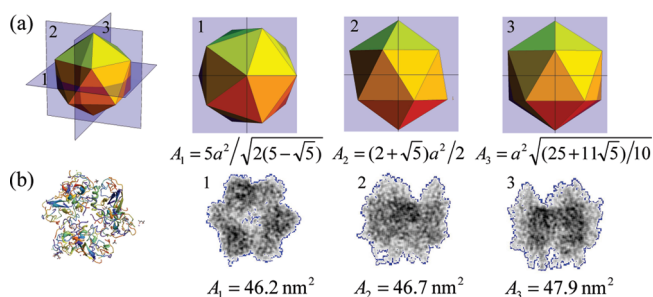


Figure 2. (a) Three orthogonal projections and projected areas for an icosahedron. (b) Ribbon diagram, three orthogonal projections and projected areas of a P3 hexamer of PRD1 consisting of three P3 proteins from the protein database.²⁷

where A_i is the projected area in each orthogonal direction, i . Figure 2a shows the three orthogonal projections for icosahedra (ideal Platonic solids) and also gives the corresponding projected area, where a represents the length of an edge between neighboring vertices. Substituting these areas into eq 2 yields $d_m \approx 1.657a$, so for PR772, $a = 36.0 \text{ nm} \pm 1.9 \text{ nm}$.

From the edge length, the opposing vertex-to-vertex (l_v), facet-to-facet (l_f), and edge-to-edge (l_e) dimensions of the virus may be calculated from the diameter of a sphere circumscribed, inscribed, and tangent to the midpoint of the edges, respectively. (Please see Scheme S-1 in the Supporting Information.) Then, $l_v = ((\phi)5^{1/2})^{1/2}a$ (the length of the 5-fold axis of symmetry), $l_f = (\phi^2/3^{1/2})a$ (the length of 3 fold axis of symmetry), and $l_e = \phi a$ (the length of 2-fold axis of symmetry), where $\phi = (1 + 5^{1/2})/2$ is the golden ratio. For PR772, $l_v = 68.4 \text{ nm} \pm 3.6 \text{ nm}$, $l_f = 54.4 \text{ nm} \pm 2.8 \text{ nm}$, and $l_e = 58.2 \text{ nm} \pm 3.0 \text{ nm}$. These results also indicate that the mobility diameter measured using ES-DMA most closely approximates the edge-to-edge length, l_e . These values differ only modestly from those for PRD1 determined by electron microscopy and X-ray imaging, which are $l_v = 69.8 \text{ nm}$, $l_f = 63.7 \text{ nm}$, and $l_e = 65.5 \text{ nm}$.¹⁹ Therefore, simply accounting for icosahedral symmetry alone can lead to a 26% difference in the estimated sizes. This result indicates that simply stating a virus diameter or a size without relating it to icosahedral lengths, as is a common practice, can introduce significant uncertainty. This analysis uncertainty, in addition to heterogeneity in sample preparation between methods, accounts for the variations in the diameter reported in the ICTV database.³⁰

The peaks in Figure 1b below 30 nm represent free capsomers or capsomer assemblies. In the course of this study, several peaks were observed as labeled in Table 1 and Figure 3. The smallest of these at 8.4 nm represents the P3 hexon. This hexon is composed of three identical P3 proteins with 120° rotational symmetry (see Figure 2). Assigning a peak in the size distribution to a specific capsomer can be made in one of two ways: by calculating the peak location using atomic coordinates in a protein data bank or by correlating with the protein's molecular weight. The mobility size of the remaining capsid proteins can be predicted from the Research Collaboratory for Structural Bioinformatics (RCSB) Protein Data Bank structures and eq 2.²⁵ A similar technique was used by Pease et al. to determine the size of antibodies, antibody aggregates, and insulin oligomers with good agreement.^{25,29} Although the data bank does not contain entries for PR772, we use the better characterized PRD1 as a surrogate. Figure 2b shows the three projections from the data bank.²⁷ Substituting the corresponding projected areas into eq 2 yields

Table 1. Identification of Peaks in Figures 1 and 3 with Sizes Predicted from Protein Data Bank Structures²⁷ and Molecular Weight Correlation¹⁷

peak (nm)	label	identification	protein data bank calculation (nm)	molecular weight correlation (nm)
8.4	f	P3 capsomer	7.73	8.95
11.2	e	P3 capsomer, dimer	10.26	11.21
13.6	d	P3 capsomer, trimer	12.20	12.79
18.6	c	partial facet		
41.4		intact capsid, +2		
51.6	b	degraded capsid, +1		
61.4	a	intact capsid, +1		

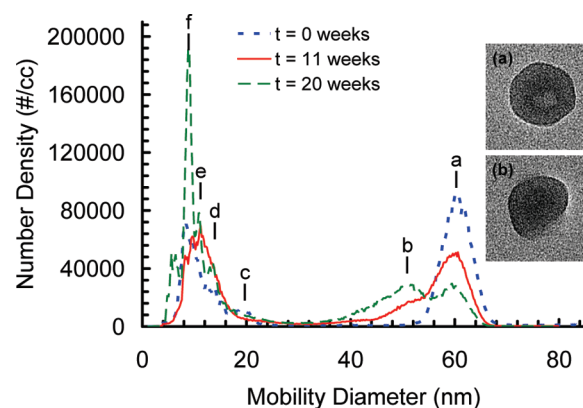


Figure 3. Serial ES-DMA size distribution of a single PR772 sample showing the disintegration of the capsid (60 nm) at $t = 0$ weeks (short dash), 11 weeks (solid), and 20 weeks (long dash) after storage at room temperature. The number density was corrected with a modified Boltzmann distribution¹⁸ to reconstruct full size distribution (not only those that acquired a positive charge in the electrospray). See Table 1 for peak identification. Insets are TEM images of representative capsids electrostatically collected at (a) 60 nm and (b) 50 nm without fixing or staining.

7.73 nm, which differs from experiment by $<1 \text{ nm}$, thereby supporting the identification. Alternatively, a correlation based on molecular weight can be used. Bacher et al. offer one such empirical correlation between molecular weight, M_w (in kg/mol), and mobility size (in nm) for globular proteins. They report $M_w = -22.033 + 9.830d_m - 1.247d_m^2 + 0.228d_m^3$. Because we seek d_m , we invert this equation to obtain $d_m = 1.832 M_w^{0.3256}$. Table 1 shows the sizes determined by this approach agree reasonably well with experimental results, perhaps because this capsomer is sufficiently globular. Indeed, the similarity in the length (8.1 nm), width (8.3 nm), and height (8.0 nm) of the P3 capsomer suggests a globular nature. Thus, both a first principles approach using the RCSB Protein Data Bank and an empirical correlation can be used to determine the identity and size of capsomers from ES-DMA data. Although the molecular weight of capsomers and capsid proteins can be obtained by several other methods, this information is readily available from ES-DMA distributions, eliminating the requirement for further gels, chromatography, or other orthogonal/complementary techniques that are less precise (fast gels), more time-consuming, or more expensive (e.g., mass spectrometry).

The above information can be used to determine viral structure. To determine the number of capsomers and proteins per

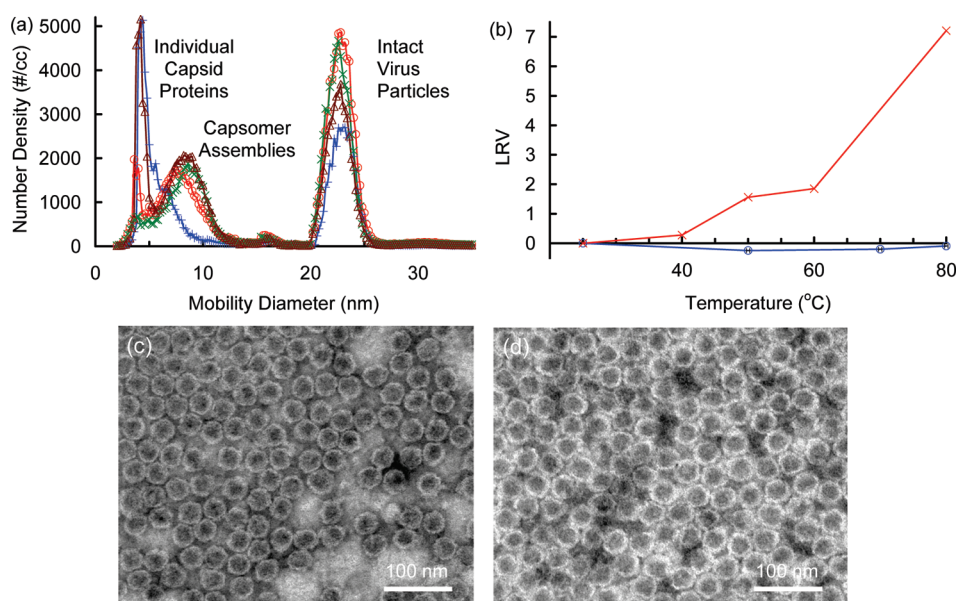


Figure 4. (a) ES-DMA size distributions for PP7 heated for 30 min to ambient ≈ 25 °C (blue +), 50 °C (red O), 70 °C (green ×), and 80 °C (brown Δ). (b) LRV versus temperature for PP7 from ES-DMA (blue O) and plaque assay (red ×). TEM images of PP7 (c) untreated and (d) heated for 30 min to 60 °C.

capsid, we make only two assumptions typical of icosahedral viruses: (1) the virus possesses an icosahedral geometry, which can be confirmed with TEM or atomic force microscopy (AFM) images (see Figure 3a), and (2) the major capsid protein forms hexons that pack hexagonally (see Scheme S-1 in Supporting Information).^{26,31} For example, with ES-DMA, we determined the edge length to be 36.0 nm (using the first assumption), and the hexon has a diameter of $8.4 \text{ nm} \pm 0.3 \text{ nm}$. Dividing the edge length by the capsomer diameter indicates that there are between 4 and 5 capsomers per edge. We note that the PR772 pentons located at the vertices of the triangle have a marginally smaller molecular weight than the hexons along the edges and in the center. Therefore, the ratio of the edge length to the hexon diameter should remain marginally less than 5. The hexons can then be arranged hexagonally as depicted in Figure S-1 (as per the second assumption). Both the number of capsomers per edge and the spatial arrangement of capsomers within the triangular face are consistent with the $T = 25$ symmetry characteristic of *Tectiviridae* and *Adenoviridae*.²⁶ Figure S-1 (see Supporting Information) then shows that 12 complete hexons can be accommodated per face, and because there are 20 faces per icosahedral capsid, the capsid contains 240 hexons of the major capsid protein. There are 12 additional pentons, one for each icosahedron vertex,³² for a total of 252 capsomers (hexons and pentons). Additionally, each of these hexons is composed of three of the major capsid proteins for a total of 720 major capsid proteins per capsid. These results determined without X-ray, neutron scattering, or electron cryomicroscopy are consistent with the known structure of *Tectiviridae* and *Adenoviridae*.^{26,31} This is an important result because we were able to confirm a key attribute of PR772 essential to its taxonomy using information collected in approximately 1 h using ES-DMA and analyzed using only two assumptions. The ease of data collection and simplicity of data analysis suggest that this technique may find broad application in structural virology.

ES-DMA can be used to not only determine intact viral structure but also investigate degradation processes (unlike X-ray

Table 2. Fraction of Particles Analyzed as Free Capsomer, Broken Capsid, and Intact Capsid

time (weeks)	free capsomer	broken capsid	intact capsid
0	39.0%	3.3%	57.7%
11	46.5%	20.9%	32.5%
20	58.9%	25.2%	15.9%

crystallography that requires diffraction through large crystals of intact virus). In Figure 3, ES-DMA size distributions of the PR772 capsid acquired as a function of storage time at room temperature are presented. Size distributions collected at 0, 11, and 20 weeks indicate significant changes in the viral structure. Initially, the size distribution consists of essentially only intact capsids and free capsomers as reported in Table 2. After 11 weeks, the magnitude of the primary capsid peak decreases by nearly half and a shoulder appears near 50 nm. Still, a majority of the protein molecules remain bound in the fully intact capsid. After 20 weeks, the primary capsid peak decreases further and the shoulder is now equal in magnitude to the primary peak. To demonstrate the utility of ES-DMA to ascertain the shelf life of viral products, we can use data in Figure 3 to calculate the rate of degradation. A simple stability metric is the half-life, which is approximately 12.8 weeks based on peak area. These data indicate the potential of ES-DMA as a tool to assess viral stability and shelf life.

In addition to the primary capsid peak, the ES-DMA size distributions contain rich information regarding the structure of degradation products. For example, we speculate that the shoulder near 50 nm may be due to partially disintegrated capsids. To test this hypothesis, we collected particles corresponding to the shoulder by dwelling at the voltage for the 50 nm size and diverting the DMA output to an electrostatic deposition chamber for several hours. The TEM images (Figure 3b and Supporting Information) clearly show an irregularly shaped capsid with curved and less distinct edges. This contrasts with particles collected at the 60 nm size (Figure 3a), which display the straight sidewalls

expected of the intact capsid. As multiple facets comprise the icosahedral capsid, removal of several of these would be necessary to produce the structure in Figure 3b. Distinguishing intact from slightly irregular capsids with ES-DMA would be useful for quality control of vaccines and gene therapy products.

Figure 3 also provides some insight into the mechanism of degradation. Initial degradation products take the form of mostly individual capsomers though some larger structures perhaps including pieces large enough to make up most of a facet (peak c) are observed. Continued loss of smaller pieces leaves partially degraded capsid (peak b). Despite the presence of metastable intermediates, the small but nonzero number density between 20 and 40 nm suggests that a continuum of breakdown products are involved in the degradation process. However, only after many weeks do the individual capsomers begin to break down as seen by the appearance of peaks <7 nm at $t = 20$ weeks. This is consistent with the unusually high stability of PRD1's P3 trimeric capsid, which Benson et al. attribute to extensive overlap between neighboring proteins.^{26,27}

We further demonstrate the potential to use ES-DMA as a tool to evaluate thermally induced degradation. In bioprocessing of therapeutic proteins, a controlled heating step can be used to disrupt capsids of any adventitious viruses in raw materials or process fluids, while retaining the 3-D structure of the protein of interest (e.g., antibodies). Figure 4 displays peaks for the bacteriophage PP7 heated to temperatures as high as 80 °C. At room temperature, only peaks corresponding to individual capsid proteins (fully dissociated at 4.2 nm) and intact virus particles are present. However, a third peak appears after heating to 50 °C, representing large capsid fragments at 15 nm. This suggests an abrupt transition in capsid integrity between 25 and 50 °C. Curiously, the diameter of the intact virus particles in Figure 4a remains between 22.8 and 23.0 nm, well within the known variability of ES-DMA measured using nanoparticles.^{6,11} Indeed, seemingly intact particles are still present in both ES-DMA distributions and TEM (Figure 4c,d) even after incubation at the highest temperatures. The simultaneous appearance of large capsid fragments and lack of change in the intact capsid peak may be reconciled if the loss of one or more of the icosahedral faces dislodges without affecting the remaining structural integrity (and thus the apparent size) of the capsid, much like shattering a single pane of glass does not affect the rest of the window. This hypothesis is further supported using an infectivity assay. Figure 4b shows that the infectivity LRV rises smartly with temperature (i.e., the infectivity goes down), indicating the loss of nucleic acid through openings in either the viral coat or partial thermal denaturation of surface loops responsible for cellular recognition. These changes are not detected by the ES-DMA, indicating that it can only detect disintegration of the external capsid (and commensurate rises in free proteins and fragments), while the infectivity assay is sensitive to other mechanisms including thermal denaturation of the protein that binds the cell to the host protein, loss of individual proteins from the capsid shell, or changes in the nucleic acids within the capsid shell.

CONCLUSION

To summarize, we have analyzed the capsid structure of the bacteriophage PR772 with ES-DMA to show it can provide structural information and track the degradation of viruses. Though outside the scope of this paper, detection of species intermediate between intact virus particles and capsomer assemblies

by ES-DMA (e.g., see Figures 3 and 4a) suggests that this technique may be able to determine the identity and concentration of intermediates in viral and macromolecular assembly processes. For example, ES-DMA may prove valuable in validating several of the models for intermediates involved in capsid assembly predicted by the recent simulations of Zandi et al. and Twarock.³³ The method's low cost relative to X-ray, neutron scattering, or electron cryomicroscopy and capability to identify quickly and accurately capsomers close in size and partially degraded capsids make it ideally suited for studying the stability and structure of complex biomolecular and virus structures.

ASSOCIATED CONTENT

S Supporting Information. Additional background regarding viral structure, additional experimental methods, capsomer packing, additional images of viral degradation, and safety considerations. This material is available free of charge via the Internet at <http://pubs.acs.org>.

AUTHOR INFORMATION

Corresponding Author

*L.F.P.: address, University of Utah, 50 S. Central Campus Drive, 3290 MEB, Salt Lake City, UT 84112; phone, 801-585-2284; fax, 801-585-9291; e-mail, pease@eng.utah.edu. M.J.T.: address, National Institute of Standards and Technology, 100 Bureau Drive, Gaithersburg, MD 20899; phone, 301-975-2609; fax, 301-975-2643, e-mail, michael.tarlov@nist.gov.

ACKNOWLEDGMENT

L.F.P. would like to acknowledge support of a postdoctoral fellowship through the National Research Council. We express appreciation for helpful suggestions and conversations with Anton P. J. Middelberg, John T. Elliott, and Kenneth D. Cole and Scott Lute (CDER/FDA) for providing the virus preps. Views expressed are not necessarily those of the FDA or the US government.

REFERENCES

- (1) Colter, J. S.; Ellem, K. A. O. *Annu. Rev. Microbiol.* **1961**, *15*, 219–244.
- (2) Casper, L. D.; Klug, A. *Cold Spring Harbor Symp. Quant. Biol.* **1962**, *27*, 1–24.
- (3) Kuzmanovic, D. A.; Elashvili, I.; O'Connell, C.; Krueger, S. *Radiat. Phys. Chem.* **2008**, *77*, 215–224.
- (4) (a) Shoemaker, G. K.; van Duijn, E.; Crawford, S. E.; Uetrecht, C.; Baclayon, M.; Roos, W. H.; Wuite, G. J.; Estes, M. K.; Prasad, B. V.; Heck, A. J. *Mol. Cell. Proteomics* **2010**, *9*, 1742–51. (b) Knapman, T. W.; Morton, V. L.; Stonehouse, N. J.; Stockley, P. G.; Ashcroft, A. E. *Rapid Commun. Mass Spectrom.* **2010**, *24*, 3033–42. (c) Kim, S. K.; Ha, T.; Schermann, J. P. *Phys. Chem. Chem. Phys.* **2010**, *12*, 13366–7.
- (5) Lute, S.; Riordan, W.; Pease III, L. F.; Tsai, D.-H.; Levy, R.; Sofer, G.; Haque, M.; Moroe, I.; Sato, T.; Morgan, M.; Krishnan, M.; Campbell, J.; Genest, P.; Dolan, S.; Meyer, A.; Zachariah, M. R.; Tarlov, M. J.; Etsel, M.; Brorson, K. *PDA J. Pharm. Sci. Technol.* **2008**, *62*, 318–333.
- (6) Pease III, L. F.; Tsai, D.-H.; Zangmeister, R. A.; Zachariah, M. R.; Tarlov, M. J. *J. Phys. Chem. C* **2007**, *111*, 17155–17157.
- (7) Mulholland, G. W.; Donnelly, M. K.; Hagwood, C. R.; Kukuck, S. R.; Hackley, V. A.; Pui, D. Y. H. *J. Res. Natl. Inst. Stand. Technol.* **2006**, *111*, 257–312.
- (8) Collins, D. R.; Cocker, D. R.; Flagan, R. C.; Seinfeld, J. H. *Aerosol Sci. Technol.* **2004**, *38*, 833–850.

- (9) Wick, C. H.; McCubbin, P. E.; Birenzvige, A. *Detection and Integration of Viruses using the Integrated Virus Detection System (IVDS)*; Edgewood, Chemical Biological Center: Edgewood, Aberdeen Proving Ground, MD, November 2005.
- (10) Thomas, J. J.; Bothner, B.; Traina, J.; Benner, W. H.; Siuzdak, G. *Spectrosc.-Int. J.* **2004**, *18*, 31–36.
- (11) Cole, K. D.; Pease III, L. F.; Tsai, D.-H.; Singh, T.; Lute, S.; Brorson, K. A.; Wang, L. *J. Chromatogr., A* **2009**, *57*, 5715–5722.
- (12) Hogan, C. J.; Kettleison, E. M.; Ramaswami, B.; Chen, D. R.; Biswas, P. *Anal. Chem.* **2006**, *78*, 844–852.
- (13) Kaddis, C. S.; Lomeli, S. H.; Yin, S.; Berhane, B.; Apostol, M. L.; Kickhoefer, V. A.; Rome, L. H.; Loo, J. A. *Am. Soc. Mass Spectrom.* **2007**, *18*, 1206–1216.
- (14) (a) Allmaier, G.; Laschober, C.; Szymanski, W. W. *Am. Soc. Mass Spectrom.* **2008**, *19*, 1062–1068. (b) Bothner, B.; Siuzdak, G. *ChemBioChem* **2004**, *5*, 258–260.
- (15) Pease III, L. F.; Lipin, D. I.; Tsai, D.-H.; Zachariah, M. R.; Lua, L. H. L.; Tarlov, M. J.; Middelberg, A. P. *J. Biotechnol. Bioeng.* **2009**, *102*, 845–855.
- (16) Siuzdak, G.; Bothner, B.; Yeager, M.; Brugidou, C.; Fauquet, C. M.; Hoey, K.; Change, C.-M. *Chem. Biol.* **1996**, *3*, 45–48.
- (17) Bacher, G.; Szymanski, W. W.; Kaufman, S. L.; Zollner, P.; Blaas, D.; Allmaier, G. *J. Mass Spectrom.* **2001**, *36*, 1038–1052.
- (18) (a) Pease III, L. F.; Tsai, D.-H.; Zangmeister, R. A.; Hertz, J. L.; Zachariah, M. R.; Tarlov, M. J. *Langmuir* **2010**, *26*, 11384–11390. (b) Wiedensohler, A. *J. Aerosol Sci.* **1987**, *19* (3), 387–389.
- (19) Lute, S.; Aranha, H.; Tremblay, D.; Liang, D. H.; Ackermann, H. W.; Chu, B.; Moineau, S.; Brorson, K. *Appl. Environ. Microbiol.* **2004**, *70*, 4864–4871.
- (20) Lute, S.; Bailey, M.; Combs, J.; Sukumar, M.; Brorson, K. A. *Biotechnol. Appl. Biochem.* **2007**, *47*, 141–151.
- (21) Kaufman, S. L. *Anal. Chim. Acta* **2000**, *406*, 3–10.
- (22) Knutson, E. O.; Whitby, K. T. *J. Aerosol Sci.* **1975**, *6*, 443–451.
- (23) Epstein, P. S. *Phys. Rev.* **1924**, *23*, 710.
- (24) Dahneke, B. E. *J. Aerosol Sci.* **1973**, *4*, 147–161.
- (25) Pease III, L. F.; Elliott, J. T.; Tsai, D. H.; Zachariah, M. R.; Tarlov, M. J. *Biotechnol. Bioeng.* **2008**, *101*, 1214–1222.
- (26) Regenmortel, M. H. V. v.; Fauquet, C. M.; Bishop, D. H. L. *Virus Taxonomy: Classification and Nomenclature of Viruses: Seventh Report of the International Committee on Taxonomy of Viruses*; Academic Press: San Diego, 2000.
- (27) Benson, S. D.; Bamford, J. K. H.; Bamford, D. H.; Burnett, R. M. *Acta Crystallogr., Sect. D: Biol. Crystallogr.* **2002**, *58*, 39–59.
- (28) (a) Stolzenburg, M. R. Ph.D. dissertation. University of Minnesota, Minneapolis, 1988. (b) Stolzenburg, M. R.; McMurry, P. H. *Aerosol Sci. Technol.* **2008**, *42*, 421–432.
- (29) Pease III, L. F.; Sorci, M.; Guha, S.; Tsai, D.-H.; Zachariah, M. R.; Tarlov, M. J.; Belfort, G. *Biophys. J.* **2010**, *99*, 3979–3985.
- (30) <http://www.ncbi.nlm.nih.gov/ICTVdb/>. Accessed 1/19/2010.
- (31) Paredes, A. M.; Brown, D. T.; Rothnagel, R.; Chiu, W.; Schoepp, R. J.; Johnston, R. E.; Prasad, B. V. V. *Proc. Natl. Acad. Sci. U.S.A.* **1993**, *90*, 9095–9099.
- (32) Casper, L. D.; Klug, A. *Cold Spring Harbor Symp. Quant. Biol.* **1962**, *27*, 1–24.
- (33) (a) Twarock, R. *Phil. Trans. R. Soc. A* **2006**, *364*, 3357–3373. (b) Zandi, R.; Reguera, D.; Bruinsma, R. F.; Gelbart, W. M.; Rudnick, J. *Proc. Natl. Acad. Sci. U.S.A.* **2004**, *101*, 15556–15560. (c) Zlotnick, A. *Proc. Natl. Acad. Sci. U.S.A.* **2004**, *101*, 15549–15550.